

Topological protection from exceptional points in Weyl and nodal line semimetals

J. González and R.A. Molina

Instituto de Estructura de la Materia, Consejo Superior de Investigaciones Científicas, Serrano 123, 28006 Madrid, Spain

(Dated: July 21, 2018)

We investigate the topological protection of surface states in Weyl and nodal-line semimetals by characterizing them as evanescent states when the band structure is extended to complex momenta. We find in this way a sequence of exceptional points—that is, branch points with zero energy in the complex spectrum—allowing us to identify the set of surface states with complex momentum signaling the decay into the 3D semimetal. From this point of view, Weyl and nodal-line semimetals can be classified in two types depending on the way surface states decay. Type A semimetals have surface states with smaller penetration length and oscillating decay while type B semimetals have longer simple exponential decays. The difference between both types reflects in the way the branch cuts in the spectrum accommodate in the complex plane. The stability of the surface states stems in this approach from the complex structure that develops around the exceptional points, with a topological protection which is based on the fact that the branch cuts cannot be closed by small perturbations. We check this property when nodal-line semimetals are placed under circularly polarized light, where we observe that the exceptional points survive the effect of such a perturbation, though appropriate boundary conditions for zero-energy surface states cannot be satisfied in general due to the breakdown of time-reversal invariance by the radiation field.

I. INTRODUCTION

Topological materials have become a primary target of research in the last few years due to their exceptional properties with high potential for applications^{1,2}. The bulk-edge correspondence and the topological protection of edge states is on the basis of the interesting properties of systems with topologically non-trivial band structure. In topological insulators, the quantity controlling the topological protection is the inverted gap between bands arising from the crystal structure of the material. A perturbation must be strong enough to close the gap in order to destroy the edge states of the material.

In band theory, a semimetal is usually defined as a material with no gap in the band structure but with a very small overlap between the valence and the conduction band, resulting in a small density of states around the Fermi energy. A typical example is bismuth which has intermediate properties between an insulator and a metal³. In topological band theory, however, it is customary to work with a more strict definition by which a semimetal is a material with no gap but also no Fermi surface, so the conduction and valence bands touch only at isolated points. The semimetal so defined is really a distinct phase intermediate between insulators and metals, the most famous example being graphene⁴. Although the Dirac nodes in the 2D Brillouin zone of graphene are not topologically protected, in three dimensions we have the last additions to the family of topological materials, which include Dirac and Weyl semimetals with isolated Dirac or Weyl nodes in the band structure^{5–8}, and the nodal-line semimetals with a continuous line of nodes in the Brillouin zone⁹.

The surface states corresponding to these topological semimetals lie on constant energy contours which do not form in general closed curves. In the case of the Weyl and Dirac semimetals, the surface states lead to the cel-

ebrated Fermi arcs joining the projection of the nodes onto the given surface. For nodal-line semimetals, the surface states form the so-called drumhead within the nodal circle^{9–11}. In the Weyl semimetals, such states are topologically protected and Chern numbers can be defined in the planes lying between Weyl nodes^{12,13}. The physical quantity measuring this protection is the separation of the nodes in momentum space. The situation is less clear for Dirac semimetals in which a simple application of bulk-surface correspondence does not provide with an answer to whether or not the surface states are topologically protected. Recent works have discussed the stability of the surface states in 3D semimetals^{14–16}. In this regard, an alternative description of the topological protection of surface states in 3D topological semimetals is very desirable. Here, we provide such a description by extending the band structure in momentum space to complex momenta.

The convenience of taking complex values of the momentum is motivated by the search of evanescent states in the 3D semimetals. When the momentum is promoted to a complex quantity, the Hamiltonian of the system becomes non-Hermitian, but it is still possible to find exceptional points in the spectrum, that is, branch points where the imaginary part of the eigenvalue vanishes. This allows one to identify the set of evanescent states with complex momentum that signals the decay into the 3D semimetal. Such states are endowed with topological protection, which arises naturally from the fact they are attached to branch cuts that cannot be removed under small perturbations. This description based on the identification between evanescent states and exceptional points was pioneered in a previous work describing surface states in Weyl semimetals in the presence of circularly polarized light¹⁷. Recently, rings of exceptional points have been also found in dissipative systems which are based on Weyl semimetals¹⁸.

When looking for evanescent states in the spectrum of the 3D semimetals, we have found that these can be classified in two different groups, depending on the pattern of the branch cuts in the plane of complex momentum. Thus, there is a class of 3D semimetals, that we denote as type A, where most part of the branch cuts run in parallel crossing the real axis. The corresponding exceptional points form then quartets belonging to the same branch of the spectrum, with each member of a quartet in a different quadrant of the complex plane. In the other class, that we denote as type B, all the branch cuts can be disposed instead along the imaginary axis, lacking the nontrivial realization of symmetry found in the type A class. From the physical point of view, this introduces also an important difference between the two classes, as the quartets found in the type A semimetals provide a higher degree of topological protection, quantified in terms of a larger length of the branch cuts and a much smaller penetration length of the evanescent states in the 3D semimetal.

Note that this classification has a different origin than the classification into type I and type II Weyl semimetals, that depends on whether the density of states vanishes at the nodal points or has some extra contributions due to the tilting of the Weyl nodes^{19,20}. Although we have only explored a model describing a type I Weyl semimetal in this work, we expect our classification to be supplementary to the classification into type I and type II Weyl semimetals, that is, we expect to be type A semimetals of type I and type II and type B semimetals also of both type I and II.

The stability of the surface states stems in our approach from the complex structure that develops for complex momentum, where different bands can be seen as different branches of the Riemann surface giving the spectrum. In this framework, a pair of exceptional points and the respective evanescent states can be only annihilated by merging the branch points, provided they lie in the same branch of the spectrum. This picture allows us to establish a connection with the usual account of the topological protection of surface states, which requires making a 2D projection of the 3D band structure to open a gap in the spectrum. In our approach a gap also exists, but this is now seen as the separation opened between different branches along a branch cut in the complex spectrum. Such a gap can be closed only as long as the exceptional points at the two ends of the branch cut are made to coalesce, which provides an alternative understanding of the topological protection in the plane of complex momentum.

In this paper we apply the complex structure developed around the exceptional points to investigate the stability of the surface states in 3D Weyl and nodal-line semimetals. We are going to see that this approach provides a very robust picture of the evanescent states in these systems. This will be checked in particular in the case of the nodal-line semimetals under circularly polarized light, which is an instructive example since that may

not be in general a small perturbation of the semimetal. We will see that the exceptional points survive indeed the effect of the electromagnetic field, though appropriate boundary conditions for surface states cannot be satisfied in general due to the breakdown of time-reversal invariance by the radiation field.

The paper is organized as follows. In Sec. II, we consider Weyl semimetals and their surface states on the light of our approach to look for evanescent states with complex momentum. Then, in Sec. III we consider nodal-line semimetals, their bulk and their surface states in cylindrical coordinates which are well-suited to the problem. In Sec. IV, we use the same approach to study the behavior of evanescent states in the case of a periodic perturbation of the nodal-line semimetal by circularly polarized light. We finish with some conclusions of our study in Sec. V.

II. WEYL SEMIMETAL

We consider a simple model for a Weyl semimetal with Hamiltonian

$$H_w = (m_0 + m_1 \nabla^2) \sigma_z - iv \partial_z \sigma_x - iv \partial_y \sigma_y. \quad (1)$$

The energy-momentum dispersion as a function of the 3D momentum \mathbf{k} is given then by

$$\varepsilon = \pm \sqrt{(m_0 - m_1 \mathbf{k}^2)^2 + v^2 k_y^2 + v^2 k_z^2}. \quad (2)$$

It turns out that the valence and conduction bands touch at Weyl points located in the line $k_y = k_z = 0$ with

$$k_x = \pm \sqrt{\frac{m_0}{m_1}}. \quad (3)$$

In this model we may look for surface states characterized by wavefunctions decaying for instance in the z direction as

$$\phi(x, y, z) \sim e^{ik_z z} e^{-\alpha z} f(x, y), \quad (4)$$

with $\alpha > 0$ corresponding to the inverse of the penetration length. The action of the Hamiltonian becomes particularly simple if we concentrate on the set of states

$$\phi_{k_x, k_z, +}(x, y, z) = e^{ik_x x} e^{ik_z z} e^{-\alpha z} |+\rangle \quad (5)$$

$$\phi_{k_x, k_z, -}(x, y, z) = e^{ik_x x} e^{ik_z z} e^{-\alpha z} |-\rangle \quad (6)$$

with the spinor part corresponding to the eigenvectors of σ_y

$$|+\rangle = \begin{pmatrix} 1 \\ i \end{pmatrix}, \quad |-\rangle = \begin{pmatrix} 1 \\ -i \end{pmatrix}. \quad (7)$$

We get in this way

$$H_w \phi_{k_x, k_z, +} = (m_0 - m_1(k_x^2 + k_z^2 - \alpha^2 + 2ik_z\alpha) + iv(k_z + i\alpha)) \phi_{k_x, k_z, -} \quad (8)$$

$$H_w \phi_{k_x, k_z, -} = (m_0 - m_1(k_x^2 + k_z^2 - \alpha^2 + 2ik_z\alpha) - iv(k_z + i\alpha)) \phi_{k_x, k_z, +}. \quad (9)$$

Then we can identify a collection of zero-energy modes in the set of states $\{\phi_{k_x, k_z, \pm}\}$ by canceling out the right-hand-side of Eq. (8) (assuming that $m_0 > 0, m_1 > 0, v > 0$). This leads to two types of solutions, either

$$\alpha = \frac{v}{2m_1} \quad (10)$$

$$k_z = \pm \sqrt{\frac{m_0}{m_1} - k_x^2 - \alpha^2} \quad (11)$$

or

$$\alpha = \frac{v \pm \sqrt{v^2 - 4m_1(m_0 - m_1k_x^2)}}{2m_1} \quad (12)$$

$$k_z = 0 \quad (13)$$

For a given k_x , two independent states with $\alpha > 0$ exist as long as $k_x^2 \leq m_0/m_1$. We note that the actual wave function corresponding to a surface state must be a linear combination of the solutions with + and - signs (in either (10)-(11) or (12)-(13)) in order to fulfill appropriate boundary conditions (for example in a semi-infinite plane, making the wave function to vanish at $z = 0$). This collection of evanescent states maps therefore the celebrated Fermi arcs with $|k_x| \leq \sqrt{m_0/m_1}$, which join the projection of the Weyl points onto a given surface of the semimetal.

The solution corresponding to Eqs. (10)-(11) is valid when $4m_1m_0 > v^2$. In this case, there is however a portion of the Fermi arcs, closer to the endpoints, where the states change to the form given by Eqs. (12)-(13). In the regime $4m_1m_0 < v^2$, all the states in the Fermi arcs correspond instead to this latter representation of the evanescent eigenstates. In what follows, we will see that there is indeed a clear distinction between two different types of surface states, allowing us to discern two different regimes of Weyl semimetals that we denote as type A (for $4m_1m_0 > v^2$) and type B (for $4m_1m_0 < v^2$).

In Fig. 1 we show numerical calculations for an equivalent tight-binding Hamiltonian in a slab of width $W = 1000$ nm in the z direction, for two different examples pertaining to type A and type B semimetals. The appearance of the band structure is very similar in the two regimes, with the Fermi arcs joining the projection of the Weyl nodes. However, in the type B regime ($4m_1m_0 < v^2$) the Fermi arc states have a penetration length ($1/\alpha$) that increases with the value of $|k_x|$ until it diverges at the projection of the Weyl nodes. In the type A regime ($4m_1m_0 > v^2$), the states with $k_x^2 < m_0/m_1 - v^2/4m_1^2$ have a very small penetration length $2m_1/v$ which would be typically of the order of a few unit cells in real materials. However, the probability

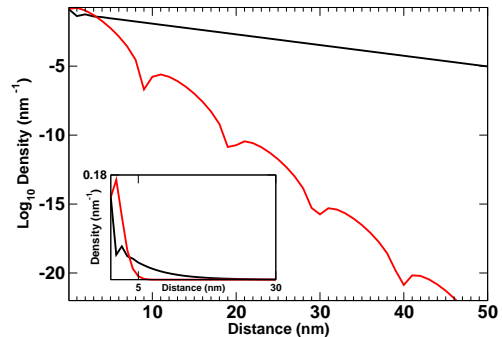


FIG. 1: Probability density in logarithmic scale across the z direction of surface states in the Fermi arcs with $k_x = 0$. We compare two different cases, one with some oscillatory dependence in the z direction corresponding to a type A Weyl semimetal (red line, $m_0 = 0.35$ eV, $m_1 = 1.0$ eV nm², $v = 1.0$ eV nm) and another with pure exponential decay corresponding to a type B Weyl semimetal (black line, $m_0 = 0.35$ eV, $m_1 = 1.0$ eV nm², $v = 4.0$ eV nm). In the inset the same figure is shown in normal scale.

density oscillates as it decays. For larger values of k_x^2 , the penetration length grows until it diverges again at the projection of the Weyl nodes, and the wave function for z is just a decaying exponential without oscillations.

Within this approach, we can also analyze the role that the evanescent states play in the spectrum of the Hamiltonian H_w , as this becomes a non-Hermitian operator acting on the basis (5)-(6). In the subspace spanned by this set of states, the eigenvalues of H_w turn out to be according to (8)-(9)

$$\lambda = \pm \sqrt{(m_0 - m_1(k_x^2 + (k_z + i\alpha)^2))^2 + v^2(k_z + i\alpha)^2} \quad (14)$$

It can be seen that the particular values satisfying the zero-mode conditions (10)-(11) and (12)-(13) correspond to branch points in the complex spectrum of H_w , both for $4m_0m_1 > v^2$ and $4m_0m_1 < v^2$. We find therefore that the evanescent states we have identified correspond to so-called exceptional points^{21,22} in the spectrum of H_w , when this is mapped as a function of the complex momentum $k_z + i\alpha$. This highlights that there is a complex structure behind the surface states of the Weyl semimetals, which has important implications for their stability.

The structure of the branch cuts in the complex plane $k_z + i\alpha$ is different however, depending on whether we consider the type A regime ($4m_0m_1 > v^2$) or the type

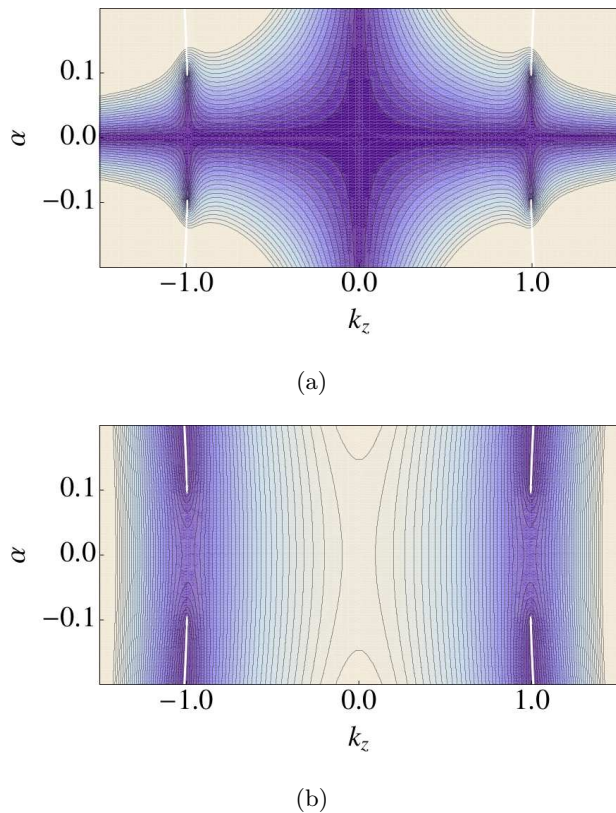


FIG. 2: Contour plots of the absolute value of the imaginary part (a) and the real part (b) of the eigenvalue in (14) for $k_x = 0$ and $m_0 = 1.0$ eV, $m_1/a^2 = 1.0$ eV, $v/a = 0.2$ eV, a being a microscopic length scale in the model. k_z and α are measured in units of a^{-1} . Lighter colors correspond to increasing energy values and dark colors represent regions close to zero.

B regime ($4m_0m_1 < v^2$) of the Weyl semimetal. In the first case, the states in the Fermi arcs with $k_x^2 < m_0/m_1 - v^2/4m_1^2$ correspond to branch points that are away from the imaginary axis, as represented in Fig. 2, where it can be observed the branch cuts that develop from the location of the zero-energy modes. The branch cuts fall eventually into the imaginary axis for $k_x^2 > m_0/m_1 - v^2/4m_1^2$, where we know that the evanescent states must be in accordance with (12)-(13). In the type B regime, however, the branch cuts are found in the imaginary axis for all the states in the Fermi arcs, with a typical structure represented in Fig. 3.

The different structure of the branch cuts in the type A and type B regimes of the Weyl semimetal can be actually ascribed to a different realization of the symmetries of the Hamiltonian (1). This is in particular invariant under the spatial inversion, which can be represented as an operator I with an action on the states $\phi(x, y, z)$ given by

$$I : \phi(x, y, z) \rightarrow \sigma_z \phi(-x, -y, -z) \quad (15)$$

The Hamiltonian (1) has moreover an enlarged symmetry when the dynamics is constrained to states that do not

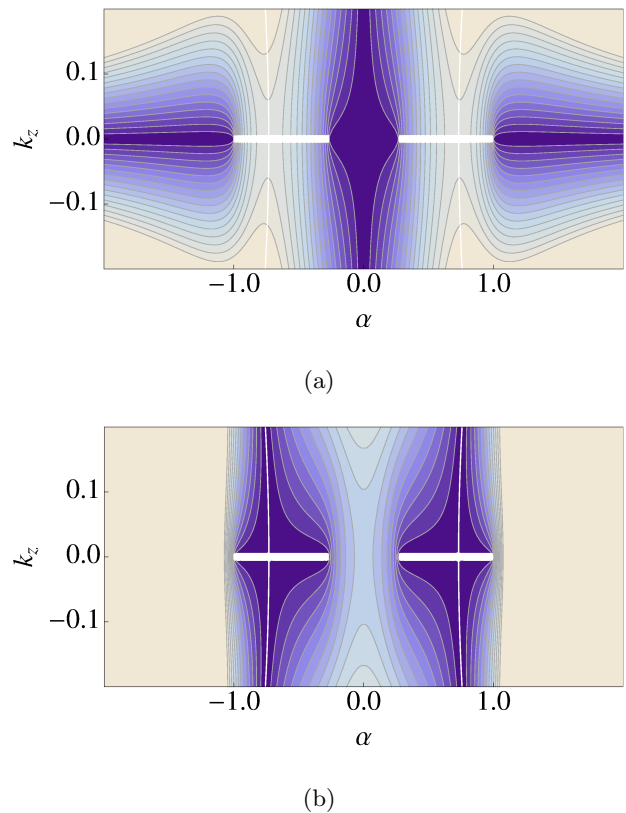


FIG. 3: Contour plots of the absolute value of the imaginary part (a) and the real part (b) of the eigenvalue in (14) for $k_x = 0$ and $m_0 = 0.5$ eV, $m_1/a^2 = 1.9$ eV, $v/a = 2.4$ eV, a being a microscopic length scale in the model. k_z and α are measured in units of a^{-1} . Lighter colors correspond to increasing energy values and dark colors represent regions close to zero.

depend on the y coordinate, as in the above discussion. Then H_w becomes invariant under a transformation T that acts like time-reversal invariance, given in terms of the operation of complex conjugation K as

$$T : \phi(x, y, z) \rightarrow K \sigma_z \phi(x, y, z) \quad (16)$$

Thus, in the structure represented in Fig. 2 for the type A regime of the Weyl semimetal, the two branch points related by the inversion of the complex momentum $k_z + i\alpha$ correspond to states that are mapped onto each other by the action of I . On the other hand, the transformation T is realized in the complex plane as the inversion $k_z \rightarrow -k_z$. This accounts for the fact that the same state $\phi(x, y, z)$ (with $y = \text{const.}$) is found at the two branch points related by such an inversion of the momentum k_z .

The fact that one finds the same evanescent state at branch points with momenta k_z and $-k_z$ is important from the point of view of the stability of the surface states. As already mentioned, two independent states $\phi(x, y, z)$ are needed in order to build a surface state that may vanish on the boundary of the system, say for instance on the plane $z = 0$. This requirement can be satis-

fied in the type A regime of the Weyl semimetal from the symmetry enforced by the T operation. Then, the surface states with $k_z \neq 0$ turn out to be protected due to the particular structure of the branch cuts, which cannot be undone unless the branch points are made to coalesce in pairs. Such kind of topological protection holds also but to a lesser degree in the type B regime of the Weyl semimetal. In that case, the evanescent states correspond to branch points with more variable separation along the imaginary axis, which can merge therefore under weaker perturbations.

We find that the exceptional points endow in general the surface states with topological protection, as the non-trivial topology of the branch cuts cannot be modified with small perturbations. When the exceptional points realize the I and T symmetry operations, that protection can be also quantified in terms of the distance separating each pair in a quartet of exceptional points. Alternatively, this protection can be also understood from the existence of a gap that opens up along each branch cut, as observed in Figs. 2 and 3, though here we realize that this is just an effect of a more involved picture relying on the full complex structure unveiled in the (k_z, α) plane.

III. NODAL LINE SEMIMETAL

A. Bulk states

Our starting point is a model of nodal line semimetal with a Hamiltonian

$$H_{\text{NL}} = (m_0 + m_1 \nabla^2) \sigma_z - iv \partial_z \sigma_x \quad (17)$$

In the case of bulk zero-energy modes, we see from (21) that they can be expressed in terms of Bessel functions J_m as

$$\psi_{0,+}^{(m)}(r, \theta, z) = e^{im\theta} J_m(kr) |u\rangle \quad (22)$$

$$\psi_{0,-}^{(m)}(r, \theta, z) = e^{im\theta} J_m(kr) |d\rangle \quad (23)$$

with $k = \sqrt{m_0/m_1}$ and the spinor part given by the eigenvectors of σ_z

$$|u\rangle = \begin{pmatrix} 1 \\ 0 \end{pmatrix}, \quad |d\rangle = \begin{pmatrix} 0 \\ 1 \end{pmatrix} \quad (24)$$

It turns out that, in this particular representation, the states corresponding to the nodal line are labeled by the

In terms of the 3D momentum \mathbf{k} , the eigenvalues of (17) are given by

$$\varepsilon = \pm \sqrt{(m_0 - m_1 \mathbf{k}^2)^2 + v^2 k_z^2} \quad (18)$$

This model has then a line of nodes in the plane $k_z = 0$, given by the circular set

$$k_x^2 + k_y^2 = \frac{m_0}{m_1} \quad (19)$$

When looking for energy eigenstates, we can concentrate on modes with well-defined angular momentum, with wavefunction ψ such that in polar coordinates (r, θ, z)

$$\psi(r, \theta, z) \sim e^{ik_z z} e^{im\theta} f(r) \quad (20)$$

The spectrum can be obtained then by solving the eigenvalue problem

$$\left[m_0 + m_1 \left(\frac{1}{r} \frac{\partial}{\partial r} \left(r \frac{\partial}{\partial r} \right) - \frac{m^2}{r^2} - k_z^2 \right) \right] \sigma_z \psi_{k_z}^{(m)} + vk_z \sigma_x \psi_{k_z}^{(m)} = \varepsilon \psi_{k_z}^{(m)} \quad (21)$$

integer values m of the projection of the angular momentum along the z direction.

B. Surface states

We are interested in surface states that take the form of evanescent waves localized at the boundary of the 3D semimetal. It can be easily seen that there is a huge set of these states characterized by the evanescence in the z direction, with wavefunction χ decaying as

$$\chi(r, \theta, z) \sim e^{ik_z z} e^{-\alpha z} e^{im\theta} f(r) \quad (25)$$

The zero-energy modes have to correspond in particular to solutions of the equation

$$\left[m_0 + m_1 \left(\frac{1}{r} \frac{\partial}{\partial r} \left(r \frac{\partial}{\partial r} \right) - \frac{m^2}{r^2} - k_z^2 + \alpha^2 - 2ik_z\alpha \right) \right] \sigma_z \chi_{k_z}^{(m)} + v(k_z + i\alpha) \sigma_x \chi_{k_z}^{(m)} = 0 \quad (26)$$

First of all, the imaginary terms must cancel out in (26). This means that the solutions must be necessarily proportional to the eigenvectors $|\pm\rangle$ of σ_y given in (7). Taking the first spinor, one obtains the constraint

$$-2im_1 k_z \alpha + ivk_z = 0 \quad (27)$$

which leads to either

$$\alpha = \frac{v}{2m_1} \quad (28)$$

or

$$k_z = 0. \quad (29)$$

Similarly to the case of the Weyl semimetals, the condition (28) gives rise to evanescent states with oscillatory decay while the condition (29) results in an exponential decay without oscillations. If we choose otherwise the second spinor in (7), that changes the sign of the last term in the left-hand-side of (26), which prevents the existence of evanescent states with $k_z \neq 0$ (for $v > 0$, $m_1 > 0$) and does not allow either to find solutions with $\alpha > 0$ when $k_z = 0$ (as we see in what follows).

Taking the value of α in (28), it turns out that the evanescent states are given by the solutions of Eq. (26)

$$\chi_{k_z,+}^{(m)}(r, \theta, z) = e^{ik_z z} e^{-\alpha z} e^{im\theta} J_m(k_r r) |\pm\rangle \quad (30)$$

with

$$k_r = \sqrt{\frac{m_0}{m_1} - k_z^2 - \alpha^2}. \quad (31)$$

If instead we adopt the condition (29), the corresponding values of α become

$$\alpha = \frac{v \pm \sqrt{v^2 - 4m_1(m_0 - m_1 k_r^2)}}{2m_1} \quad (32)$$

which implies a penetration length $1/\alpha$ diverging at the line of nodes. The relation (31) only makes sense if $4m_0 m_1 > v^2$, while in the regime $4m_0 m_1 < v^2$ all the evanescent states are found using (32). As in the case of the Weyl semimetal, this disjunctive allows us to distinguish between two different classes of nodal line semimetals, that we denote as type A (for $4m_0 m_1 > v^2$) and type B (for $4m_0 m_1 < v^2$). The type A corresponds to the regime that is expected to hold for realistic materials providing examples of nodal line semimetals. From the physical point of view, the two classes A and B can be discerned by the different penetration of the drumhead surface states into the material, which shows for a slab practically the same behavior as represented in the case of the Weyl semimetal in Fig. 1.

From a formal point of view, the difference between type A and type B nodal line semimetals lies in the distinctive complex structures that develop in the plane (k_z, α) . In a type A nodal line semimetal which has for instance a finite circular section at the boundary $z = 0$, the values of k_r become quantized, which turns into the consequent quantization of the momentum k_z . It can be seen that the allowed values of $k_z + i\alpha$ leading to evanescent states emerge then as exceptional points in the extension of the momentum k_z to the complex plane, as represented in Fig. 4. Those can be characterized indeed as branch points in the spectrum of the Hamiltonian for complex momentum, leading to branch cuts that run down to homologous branch points with the reversed sign of α .

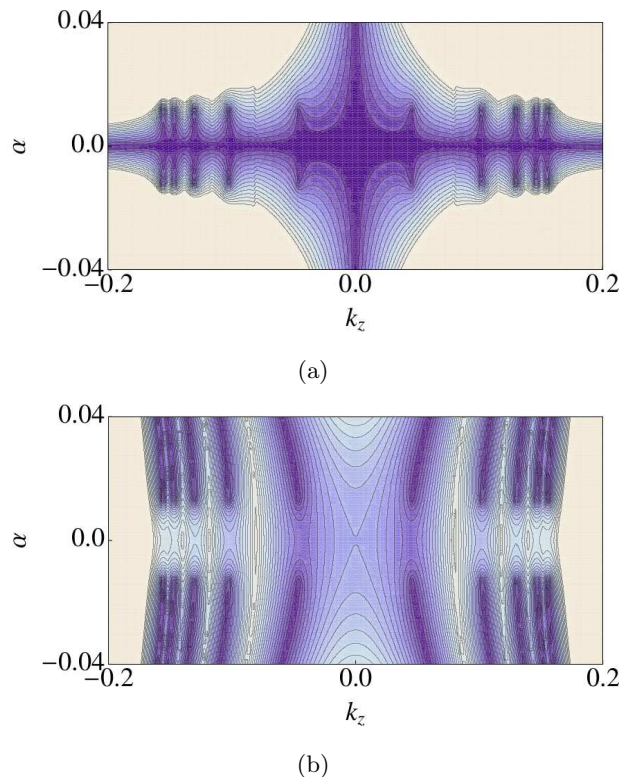


FIG. 4: Contour plots of the absolute value of the imaginary part (a) and the real part (b) of the lowest eigenvalue in the spectrum of H_{NL} for evanescent states with angular momentum $m = 0$ in a semi-infinite cylindrical geometry with radius $R = 100a$ (a being the microscopic length scale in the model), for $m_0 = 0.1$ eV, $m_1/a^2 = 4.0$ eV, $v/a = 0.1$ eV. The units and the intensity code are the same as in Fig. 2.

We observe in Fig. 4 that the exceptional points can be grouped forming quartets, which is a consequence of the

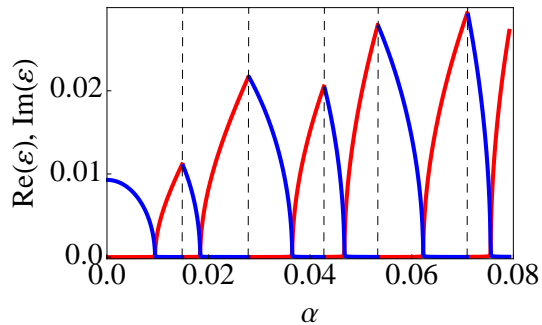


FIG. 5: Plot of the absolute value of the real part (blue lines) and the imaginary part (red lines) of the lowest eigenvalue in the spectrum of H_{NL} for evanescent states with angular momentum $m = 0$ in a semi-infinite cylindrical geometry with radius $R = 100a$ (a being the microscopic length scale in the model), for $m_0 = 0.1$ eV, $m_1/a^2 = 2.0$ eV, $v/a = 1.0$ eV. The units are the same as in Fig. 2.

invariance of the Hamiltonian (17) under the operations defined by (15) and (16). We have actually

$$[H_{\text{NL}}, I] = 0 \quad (33)$$

$$[H_{\text{NL}}, T] = 0 \quad (34)$$

The invariance under T is responsible for the fact that each pair of evanescent states with opposite sign of k_z may have the same wavefunction at $z = 0$. This symmetry is crucial in order to enforce the boundary conditions for the surface states at the edge of the semimetal, allowing to build for instance linear combinations of evanescent states that vanish at $z = 0$. Moreover, the stability of the surface states is also guaranteed by the separation in the (k_z, α) plane between evanescent states related by the I and T operations, which lend topological protection as the branch cuts running between the respective branch points cannot be closed under small perturbations.

Such a nontrivial realization of the invariance under I and T holds only in the case of the type A nodal line semimetal, as for type B all the evanescent states have $k_z = 0$. In this latter case, they correspond to exceptional points in the spectrum of H_{NL} which fall along the imaginary axis in the (k_z, α) complex plane. A representation of the sequence of branch points for a type B nodal line semimetal with cylindrical geometry is shown in Fig. 5. We notice that the plot has a series of discontinuities, which arise from the fact that the lowest eigenvalue of H_{NL} is found in different subbands as the value of α increases. In each continuous region, we observe a clear characterization of the branch point as the location where the real and the imaginary part of the eigenvalue vanish.

The plot in Fig. 5 highlights an important property that applies both to type A and type B nodal line semimetals. As already mentioned, it is clearly observed in the figure that exceptional points with different values

of the complex momentum belong in general to different subbands in the spectrum of H_{NL} . This can be also appreciated (though less neatly) in the representation of Fig. 4, where a careful inspection shows that a line of discontinuity exists in the contour plot between each two consecutive branch cuts. From the point of view of the complex structure, this means that exceptional points with different values of $k_z + i\alpha$ belong in general to different branches of the Riemann sheet arising from the diagonalization of H_{NL} for complex momentum. This implies that it is not possible in general to undo the branch cuts by merging contiguous exceptional points. The only branch points that can be made to coalesce are those that pertain to the same branch in the complex structure—which, in the case of a type A semimetal, are those connected precisely by the I and T operations. This reassures once more the topological stability of the collection of drumhead surface states, implied in this framework by the underlying complex structure of the spectrum.

IV. EVANESCENT STATES IN NODAL LINE SEMIMETAL UNDER ELECTROMAGNETIC RADIATION

A very interesting line of research is the control of quantum properties by external ac fields^{23–28}. In this search, it has been found that the effect of electromagnetic radiation may change the properties of 2D semimetals, opening a gap in the bulk and leading to chiral currents at the boundary of the electron system^{29–35}. The effect of the radiation has been also investigated in the case of 3D Dirac and Weyl semimetals, finding that a circularly polarized photon field has the ability to shift the Dirac or Weyl points in momentum space^{36–38}. New surface states have been also discovered in Weyl semimetals illuminated by monochromatic radiation, forming bands with macroscopic degeneracy and rotating currents¹⁷. Another interesting result is that, using circularly polarized light in the proper direction, a nodal line semimetal can be transformed into a Weyl semimetal³⁹.

In this section, we show that the idea of describing the surface states by exceptional points in the spectrum can be generalized to the case of the nodal line semimetals under electromagnetic radiation. This is a relevant instance to check the topological protection that arises when extending the momenta to the complex plane, since the effects of the radiation can be studied in regimes where it is not a small perturbation.

The coupling to the vector potential can be done in the usual fashion, adopting the Peierls prescription $\mathbf{k} \rightarrow \mathbf{k} + \mathbf{A}$. In the case of circularly polarized radiation sent along the z direction, we have

$$\mathbf{A} = (A \cos(\Omega t), A \sin(\Omega t), 0) \quad (35)$$

The Hamiltonian becomes then

$$H = (m_0 + m_1(\partial_x^2 + \partial_y^2 + 2iA \cos(\Omega t)\partial_x + 2iA \sin(\Omega t)\partial_y - A^2 + \partial_z^2)) \sigma_z - iv\partial_z\sigma_x \quad (36)$$

$$= (m_0 + m_1(\partial_x^2 + \partial_y^2 + iAe^{i\Omega t}\partial_- + iAe^{-i\Omega t}\partial_+ - A^2 + \partial_z^2)) \sigma_z - iv\partial_z\sigma_x \quad (37)$$

with

$$\partial_- = \partial_x - i\partial_y \quad (38)$$

$$\partial_+ = \partial_x + i\partial_y \quad (39)$$

We have the commutation rules with the angular momentum $L_z = -ix\partial_y + iy\partial_x$:

$$[L_z, \partial_-] = -\partial_- \quad (40)$$

$$[L_z, \partial_+] = \partial_+ \quad (41)$$

$$U = e^{-iL_z\Omega t} \quad (44)$$

From these relations, it can be easily seen that

$$e^{iL_z\Omega t} \partial_- e^{-iL_z\Omega t} = e^{-i\Omega t} \partial_- \quad (42)$$

$$e^{iL_z\Omega t} \partial_+ e^{-iL_z\Omega t} = e^{i\Omega t} \partial_+ \quad (43)$$

We can now rely on Eqs. (42)-(43) to pass to a time-independent Hamiltonian by applying the unitary transformation

We have

$$\tilde{H} = U^\dagger H U - iU^\dagger \partial_t U = (m_0 + m_1(\partial_x^2 + \partial_y^2 + iA\partial_- + iA\partial_+ - A^2 + \partial_z^2)) \sigma_z - iv\partial_z\sigma_x - \Omega L_z \quad (45)$$

We can now perform an analysis of the evanescent states under radiation, following that accomplished before for the Hamiltonian H_{NL} . The idea is to focus on evanescent states decaying as

$$\chi(r, \theta, z) \sim e^{ik_z z} e^{-\alpha z} f(r, \theta) \quad (46)$$

We look in particular for zero-energy modes, which must correspond to solutions of the equation

$$\left[m_0 + m_1 \left(\frac{1}{r} \frac{\partial}{\partial r} \left(r \frac{\partial}{\partial r} \right) + \frac{\partial_\theta^2}{r^2} + iA\partial_- + iA\partial_+ - A^2 - k_z^2 + \alpha^2 - 2ik_z\alpha \right) \right] \sigma_z \chi_{k_z} + v(k_z + i\alpha) \sigma_x \chi_{k_z} + i\Omega \partial_\theta \chi_{k_z} = 0 \quad (47)$$

We perform first a numerical analysis of the problem, in which it is convenient to apply the gauge transformation

$$\chi_{k_z} = e^{-iAx} \tilde{\chi}_{k_z} \quad (48)$$

This converts Eq. (47) into

$$\left[m_0 + m_1 \left(\frac{1}{r} \frac{\partial}{\partial r} \left(r \frac{\partial}{\partial r} \right) + \frac{\partial_\theta^2}{r^2} - k_z^2 + \alpha^2 - 2ik_z\alpha \right) \right] \sigma_z \tilde{\chi}_{k_z} + v(k_z + i\alpha) \sigma_x \tilde{\chi}_{k_z} + i\Omega \partial_\theta \tilde{\chi}_{k_z} - A\Omega r \sin(\theta) \tilde{\chi}_{k_z} = 0 \quad (49)$$

Then one can check that it is possible to adjust the val-

ues of k_z and α to obtain solutions of Eq. (49). The

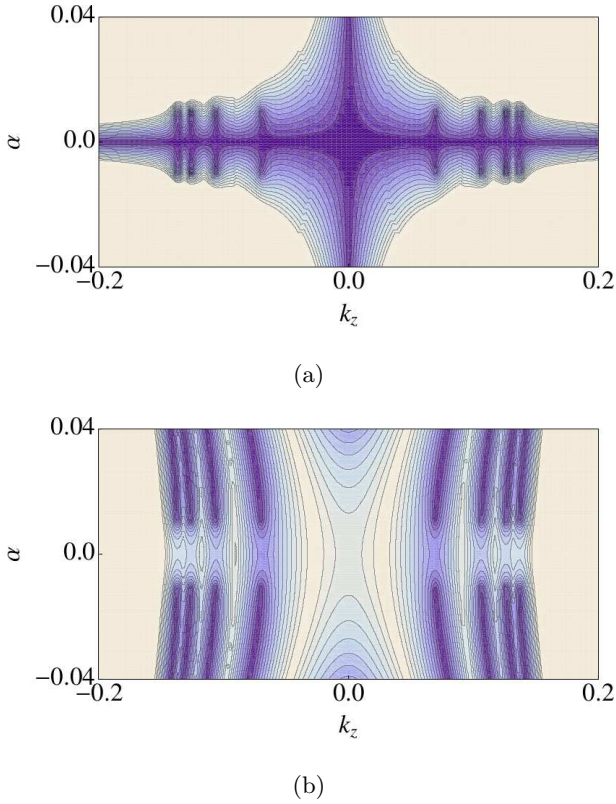


FIG. 6: Contour plots of the absolute value of the imaginary part (a) and the real part (b) of the lowest eigenvalue in the spectrum of \tilde{H} for evanescent states in a semi-infinite cylindrical geometry with radius $R = 100a$ (a being the microscopic length scale in the model) for $m_0 = 0.01$ eV, $m_1/a^2 = 0.5$ eV, $v/a = 0.01$ eV, $Aa = 0.05$, $\Omega = 1.0$ eV. The units and intensity code are the same as in Fig. 2.

numerical resolution can be done for instance in a cylinder with $r < R$, in which there is a finite number of solutions depending on the radius R . These can be more easily visualized computing the spectrum of the operator

$$\tilde{H}\chi_{k_z,+}^{(m)} = im_1A\hat{k}_r\chi_{k_z,-}^{(m-1)} - im_1A\hat{k}_r\chi_{k_z,-}^{(m+1)} + m_1\delta^2\chi_{k_z,-}^{(m)} - (v\alpha + i(2m_1\alpha - v)k_z)\chi_{k_z,-}^{(m)} - m\Omega\chi_{k_z,+}^{(m)} \quad (55)$$

$$\tilde{H}\chi_{k_z,-}^{(m)} = im_1A\hat{k}_r\chi_{k_z,+}^{(m-1)} - im_1A\hat{k}_r\chi_{k_z,+}^{(m+1)} + m_1\delta^2\chi_{k_z,+}^{(m)} - (-v\alpha + i(2m_1\alpha + v)k_z)\chi_{k_z,+}^{(m)} - m\Omega\chi_{k_z,-}^{(m)} \quad (56)$$

One can check that, for not too large values of k_z and A , it is possible to find a point in the space of parameters (α, δ) where the eigenvalue of \tilde{H} becomes zero. This arises as a branch point in the spectrum of complex eigenvalues, as represented in Fig. 7. This procedure works up to certain limit values of A and k_z , beyond which the branch point is lost and there is no signature of zero-energy modes.

in Eq. (49) in the complex plane (k_z, α) , which leads in general to a picture like that represented in Fig. 6.

We observe that the zero-energy modes correspond once again to exceptional points in a spectrum of complex eigenvalues, with a structure similar to that already found in the absence of electromagnetic radiation. The exceptional points are easily identified as branch points with a tail where the lowest eigenvalue has zero imaginary part, and an opposite tail where the real part of the eigenvalue vanishes. This is the typical behavior for a square root singularity, which is also consistent with the structure of the branch cuts connecting homologous branch points across the k_z axis, as seen in Fig. 6.

We can complement the numerical approach with an analytic search of the solutions of Eq. (47) when the surface has infinite size. We can start with the set of states spanned by the basis

$$\chi_{k_z,+}^{(m)}(r, \theta, z) = e^{ik_z z} e^{-\alpha z} e^{im\theta} J_m(\hat{k}_r r) |+\rangle \quad (50)$$

$$\chi_{k_z,-}^{(m)}(r, \theta, z) = e^{ik_z z} e^{-\alpha z} e^{im\theta} J_m(\hat{k}_r r) |-\rangle \quad (51)$$

where

$$\hat{k}_r = \sqrt{\frac{m_0}{m_1} - k_z^2 + \alpha^2 - A^2 - \delta^2} \quad (52)$$

In this case, we keep α and δ as free parameters that we have to adjust in order to find the solutions of Eq. (47). This provides us with a very flexible collection of states, which proves to be large enough to capture the evanescent zero-energy modes.

The action of the off-diagonal perturbations induced in (47) by the radiation is given by

$$\partial_- \sigma_z \chi_{k_z,\pm}^{(m)} = \hat{k}_r \chi_{k_z,\mp}^{(m-1)} \quad (53)$$

$$\partial_+ \sigma_z \chi_{k_z,\pm}^{(m)} = -\hat{k}_r \chi_{k_z,\mp}^{(m+1)} \quad (54)$$

Then, the states we obtain by the action of \tilde{H} remain in the subspace we have defined:

If we plot the spectrum as a function of $k_z + i\alpha$, once the appropriate value of δ is set, we get the image shown in Fig. 8. We observe there a line of zero-energy modes, which may be thought as the accumulation of the exceptional points already found in the finite-size numerical approach. This shows that a continuum of evanescent modes persist under the effect of the electromagnetic radiation, arising as a result of the hybridization of drum-

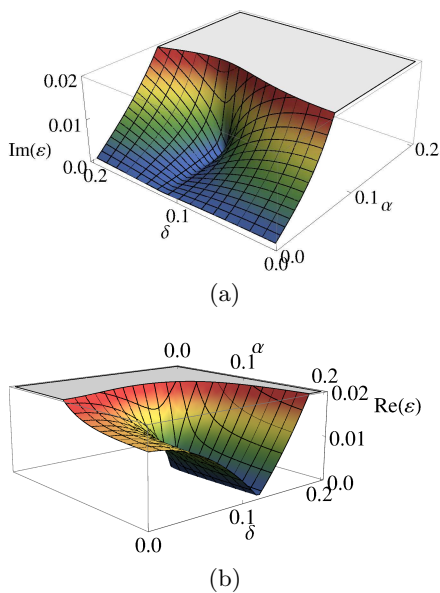


FIG. 7: Plot of the absolute value of the imaginary part (a) and the real part (b) of the lowest eigenvalue of \tilde{H} for evanescent states with variable parameters α and δ , for $k_z a = 0.2$ and $m_0 = 1.0$ eV, $m_1/a^2 = 1.0$ eV, $v/a = 0.2$ eV, $Aa = 0.1$, $\Omega = 0.5$ eV. The units are the same as in Fig. 2.

head states with different angular momentum and being labeled by the component k_z of the momentum.

We have to remark however that, in the present case, the exceptional points we have found do not imply the existence of zero-energy surface states attached to a given boundary of the nodal line semimetal. This is so as the evanescent eigenstates of \tilde{H} do not realize the symmetry required to build appropriate linear combinations that may guarantee the vanishing of the surface states at the boundary, say at $z = 0$. In the case of the unperturbed nodal line semimetal, we saw above that the crucial symmetry for the existence of zero-energy surface states was given by the T operation in (16). The introduction of the radiation field breaks the time-reversal invariance, which explains that the evanescent modes corresponding to momenta k_z and $-k_z$ have different wave functions at $z = 0$ in the presence of the radiation. This stresses the significance of the symmetry of the Hamiltonian to guarantee the stability of the zero-energy surface states, together with the topological protection already provided by the existence of the exceptional points in the spectrum.

V. CONCLUSIONS

We have shown how the surface states in topological semimetals are associated to exceptional points of the spectrum in the extension of the Brillouin zone to complex values of momenta. These exceptional points are very robust under perturbations of the Hamiltonian as

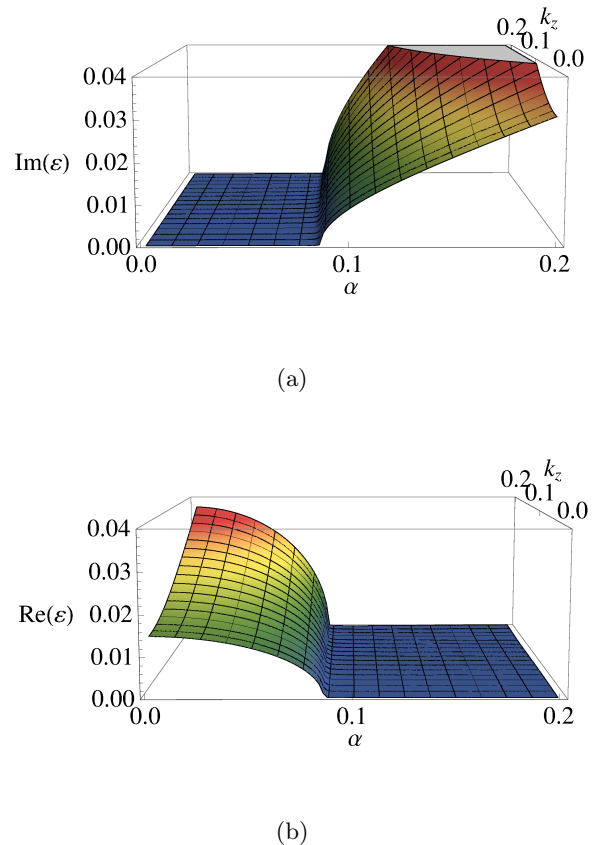


FIG. 8: Plot of the absolute value of the imaginary part (a) and the real part (b) of the lowest eigenvalue of \tilde{H} for evanescent states with complex momentum $k_z + i\alpha$, for $m_0 = 1.0$ eV, $m_1/a^2 = 1.0$ eV, $v/a = 0.2$ eV, $Aa = 0.1$, $\Omega = 0.5$ eV. The units are the same as in Fig. 2.

they can be only annihilated by merging them in pairs to close the branch cuts in the spectrum. This draws a useful way of understanding the topological protection of evanescent states like those forming the Fermi arcs in Weyl semimetals or the drumhead states in nodal line semimetals. In this regard, the mechanism of topological protection seems to be rather different to that of the nodes of the semimetals themselves (and different also to that studied recently in the case of 3D Dirac semimetals¹⁴).

We have also shown that the evanescent states decay exponentially into the semimetal, and we have illustrated the dependence of the penetration length according to the parameters of a model Hamiltonian for both Weyl and nodal line semimetals. The penetration into the semimetal can be very short and oscillating, or longer and with pure exponential decay, depending on the ratio between the linear and the quadratic terms in the Hamiltonian. According to this ratio, we have classified the topological semimetals as type A or type B. Although

we expect the type A (the short penetration with oscillations) to be realized in real materials, the proposals for artificial topological semimetals in photonic or cold atom setups could easily reach both regimes^{40–43}. The distinction between type A and type B is also formally related to the different way in which the branch cuts corresponding to the exceptional points are arranged in the complex plane.

In nodal line semimetals, we have also studied the effect of an external ac field on the surface states. Evanescent states with different angular momentum are mixed by the external field. Interestingly, the resulting states are still in correspondence to exceptional points in the complex plane and they are protected from small perturbations as such. These mixtures of states with different angular momenta should carry a rotating current similarly to that studied before in Weyl semimetals¹⁷. However, the reduction of symmetry from the ac field implies that the zero-energy surface states of nodal line semimetals are in general not stable in the presence of radiation, as this breaks the required invariance to comply with appropriate boundary conditions.

We believe our work paves the way for an alternative understanding of topological protection of edge states in gapless systems, based on the extension of the band structure for complex values of the momenta. In this complex momentum space, the surface states arise as exceptional points, making possible to study their stability by discerning the perturbations capable to close the branch cuts in the complex band structure. It would be an interesting future avenue to investigate the connection between this description of surface states and the topological properties of photonic materials or open quantum systems that can be described by actual non-Hermitian Hamiltonians^{44–48}.

Acknowledgments

We acknowledge financial support through Spanish grants MINECO/FEDER No. FIS2015-63770-P and No. FIS2014-57432-P.

-
- ¹ M. Z. Hasan and C. L. Kane, Topological insulators, *Rev. Mod. Phys.* **82**, 3045 (2010).
 - ² X.-L. Qi and S.-C. Zhang, Topological insulators and superconductors, *Rev. Mod. Phys.* **83**, 1057 (2011).
 - ³ G. Burns, *Solid State Physics* (Academic Press, New York, 1985).
 - ⁴ K. S. Novoselov, A. K. Geim, S. V. Morozov, D. Jiang, Y. Zhang, S. V. Dubonos, I. V. Grigorieva, and A. A. Firsov, Electric field effect in atomically thin carbon films, *Science* **306**, 666 (2004).
 - ⁵ Z. K. Liu, B. Zhou, Y. Zhang, Z. J. Wang, H. M. Weng, D. Prabhakaran, S.-K. Mo, Z. X. Shen, Z. Fang, X. Dai, Z. Hussain and Y. L. Chen, Discovery of a Three-Dimensional Topological Dirac Semimetal, Na_3Bi , *Science* **343**, 864 (2014).
 - ⁶ M. Neupane, S. Xu, R. Sankar, N. Alidoust, G. Bian, C. Liu, I. Belopolski, T.-R. Chang, H.-T. Jeng, H. Lin, A. Bansil, F. Chou and M. Z. Hasan, Observation of a three-dimensional topological Dirac semimetal phase in high-mobility Cd_3As_2 , *Nature Commun.* **5**, 3786 (2014).
 - ⁷ S. Borisenko, Q. Gibson, D. Evtushinsky, V. Zabolotnyy, B. Büchner and R. J. Cava, Experimental realization of a three-dimensional Dirac semimetal, *Phys. Rev. Lett.* **113**, 027603 (2014).
 - ⁸ S.-Y. Xu, I. Belopolski, N. Alidoust, M. Neupane, G. Bian, C. Zhang, R. Sankar, G. Chang, Z. Yuan, C.-C. Lee, S.-M. Huang, H. Zheng, J. Ma, D. S. Sanchez, B. Wang, A. Bansil, F. Chou, P. P. Shibayev, H. Lin, S. Jia, and M. Z. Hasan, Discovery of a Weyl fermion semimetal and topological Fermi arcs, *Science* **349**, 613 (2015).
 - ⁹ A.A. Burkov, Topological Semimetals, *Nat. Materials* **15**, 1145 (2016).
 - ¹⁰ M. Phillips, V. Aji, Tunable line node semimetals. *Phys. Rev. B* **90**, 115111 (2014).
 - ¹¹ C. Chiu, A. Schnyder, Classification of reflection symmetry protected topological semimetals and nodal superconductors. *Phys. Rev. B* **90**, 205136 (2014).
 - ¹² X. Wan, A.M. Turner, A. Vishwanath, S.Y. Savrasov, Topological semimetal and fermi-arc surface states in the electronic structure of pyrochlore iridates, *Phys. Rev. B* **83**, 205101 (2011).
 - ¹³ K.Y. Yang, Y.M. Lu, Y. Ran, Quantum Hall effects in a Weyl semimetal: Possible application in pyrochlores iridates, *Phys. Rev. B* **84**, 075129 (2011).
 - ¹⁴ M. Kargarina, M. Randeria, Y.-M. Lu, Are the surface Fermi arcs in Dirac semimetals topologically protected?, *PNAS* **113**, 8648 (2016).
 - ¹⁵ E. V. Gorbar, V. A. Miransky, I. A. Shovkovy, and P. O. Sukhachov, Surface Fermi arcs in \mathbb{Z}_2 Weyl semimetals $A_3\text{Bi}$ ($A = \text{Na, K, Rb}$), *Phys. Rev. B* **91**, 235138 (2015); Dirac semimetals $A_3\text{Bi}$ ($A = \text{Na, K, Rb}$) as \mathbb{Z}_2 Weyl semimetals, *Phys. Rev. B* **91**, 121101(R) (2015).
 - ¹⁶ S. Tchoumakov, M. Civelli, and M. O. Goerbig, Magnetic description of the Fermi arc in type-I and type-II Weyl semimetals, arXiv:1612.07693 (to appear in *Phys. Rev. B*).
 - ¹⁷ J. González and R.A. Molina, Macroscopic degeneracy of zero-mode rotating surface states in 3D Dirac and Weyl semimetals under radiation, *Phys. Rev. Lett.* **116**, 156803 (2016).
 - ¹⁸ Y. Xu, S.-T. Wang, and L.-M. Duan, Weyl Exceptional Rings in a Three-Dimensional Dissipative Cold Atomic Gas, *Phys. Rev. Lett.* **118**, 045701 (2017).
 - ¹⁹ A.A. Soluyanov, D. Gresch, Z. Wang, Q. Wu, M. Troyer, X. Dai, B.A. Bernevig, Type-II Weyl semimetals, *Nature* **527**, 495 (2015).
 - ²⁰ Y. Xu, F. Zhang, and C. Zhang, Structured Weyl Points in Spin-Orbit Coupled Fermionic Superfluids, *Phys. Rev. Lett.* **115**, 265304 (2015).
 - ²¹ M. V. Berry, Physics of non-Hermitian degeneracies, *Czech. J. Phys.* **54**, 1039 (2004).

- ²² W. D. Heiss, The physics of exceptional points, *J. Phys. A: Math. Theor.* **45**, 444016 (2012).
- ²³ D.H. Dunlap and V.M. Kenkre, Dynamic localization of a charged particle moving under the influence of an electric field, *Phys. Rev. B* **34**, 3625 (1986).
- ²⁴ F. Grossmann, T. Dittrich, P. Jung, P. Hänggi, Coherent destruction of tunneling, *Phys. Rev. Lett.* **67**, 516 (1991).
- ²⁵ M. Holthaus, G.H. Ristow, D.W. Hone, ac-Field-Controlled Anderson Localization in Disordered Semiconductor Superlattices, *Phys. Rev. Lett.* **75**, 3914 (1995).
- ²⁶ G. Platero, R. Aguado, Photon-assisted transport in semiconductor nanostructures, *Phys. Rep.* **395**, 1 (2004).
- ²⁷ D.F. Martinez, R.A. Molina, Delocalization induced by low-frequency driving in disordered tight-binding lattices, *Phys. Rev. B* **73**, 073104 (2006).
- ²⁸ C.E. Creffield, Quantum control and entanglement using periodic driving fields, *Phys. Rev. Lett.* **99**, 110501 (2007).
- ²⁹ T. Oka and H. Aoki, Photovoltaic Hall effect in graphene, *Phys. Rev. B* **79**, 081406 (2009).
- ³⁰ N. H. Lindner, G. Refael, and V. Galitski, Floquet topological insulators, *Nature Phys.* **7**, 490 (2011).
- ³¹ J.-I. Inoue and A. Tanaka, Photoinduced transition between conventional and topological insulators in two-dimensional electronic systems, *Phys. Rev. Lett.* **105**, 017401 (2010).
- ³² T. Kitagawa, E. Berg, M. Rudner, and E. Demler, Topological characterization of periodically driven quantum systems, *Phys. Rev. B* **82**, 235114 (2010).
- ³³ T. Kitagawa, T. Oka, A. Brataas, L. Fu, and E. Demler, Transport properties of nonequilibrium systems under the application of light: Photoinduced quantum Hall insulators without Landau levels, *Phys. Rev. B* **84**, 235108 (2011).
- ³⁴ Z. Gu, H. A. Fertig, D. P. Arovas, and A. Auerbach, Floquet spectrum and transport through an irradiated graphene ribbon, *Phys. Rev. Lett.* **107**, 216601 (2011).
- ³⁵ A. Gómez-León, G. Platero, Floquet-Bloch theory and topology in periodically-driven lattices, *Phys. Rev. Lett.* **110**, 200403 (2013).
- ³⁶ R. Wang, B. Wang, R. Shen, L. Sheng, D. Y. Xing, Floquet Weyl semimetal induced by off-resonant light, *Europhys. Lett.* **105**, 17004 (2014).
- ³⁷ A. Narayan, Floquet dynamics in two-dimensional semi-Dirac semimetals and three-dimensional Dirac semimetals, *Phys. Rev. B* **91**, 205445 (2015).
- ³⁸ C.-K. Chan, P. A. Lee, K. S. Burch, J. H. Han, and Y. Ran, When chiral photons meet chiral fermions - photoinduced anomalous Hall effects in Weyl semimetals, *Phys. Rev. Lett.* **116**, 026805 (2016).
- ³⁹ Z. Yan, Z. Wang, Tunable Weyl Points in Periodically Driven Nodal Line Semimetals, *Phys. Rev. Lett.* **117**, 087402 (2016).
- ⁴⁰ T. Dubcek, C.J. Kennedy, L. Lu, W. Ketterlee, M. Soljačić, and H. Buljan, Weyl points in three-dimensional optical lattices: synthetic magnetic monopoles in momentum space, *Phys. Rev. Lett.* **114**, 225301 (2015).
- ⁴¹ Y. Xu and C. Zhang, Dirac and Weyl rings in three-dimensional cold-atom optical lattices, *Phys. Rev. A* **93**, 063606 (2016).
- ⁴² L. Lu, L. Fu, J.D. Joannopoulos, M. Soljačić, Weyl points and line nodes in gyroid photonic crystals, *Nat. Photonics* **7**, 294 (2013).
- ⁴³ L. Lu, Z. Wang, D. Ye, L. Ran, L. Fu, J.D. Joannopoulos, M. Soljačić, Experimental observation of Weyl points, *Science* **349**, 622 (2015).
- ⁴⁴ K. Esaki, M. Sato, K. Hasebe, M. Kohmoto, Edge states and topological phases in non-Hermitian systems, *Phys. Rev. B* **84**, 205128 (2011).
- ⁴⁵ S. Diehl, E. Rico, M.A. Baranov, P. Zoller, Topology by dissipation in atomic quantum wires, *Nat. Phys.* **7**, 971 (2011).
- ⁴⁶ J.M. Zeuner, M.C. Rechtsman, Y. Plotnik, Y. Lumer, S. Nolte, M.S. Rudner, M. Segev, A. Szameit, Observation of a Topological Transition in the Bulk of a Non-Hermitian System, *Phys. Rev. Lett.* **116**, 040402 (2016).
- ⁴⁷ P. San-José, J. Cayao, E. Prado, R. Aguado, Majorana bound states from exceptional points in non-topological superconductors, *Sci. Rep.* **6**, 21427 (2016).
- ⁴⁸ B. Peng, S. K. Özdemir, M. Liertzer, W. Chen, J. Kramer, H. Yilmaz, J. Wiersig, S. Rotter, L. Yang, Chiral modes and directional lasing at exceptional points, *PNAS* **113**, 6845 (2016).